



# Preparation of graphene film reinforced CoCrFeNiMn high-entropy alloy matrix composites with strength-plasticity synergy via flake powder metallurgy method

Chongyang Liu<sup>a,b</sup>, Xiaosong Jiang<sup>a,b,\*</sup>, Hongliang Sun<sup>a,b</sup>, Tianyan Liu<sup>c,\*\*</sup>, Zixuan Wu<sup>d</sup>, Liu Yang<sup>e</sup>

<sup>a</sup> Key Laboratory of Advanced Technologies of Materials, Ministry of Education, Chengdu, 610031, China

<sup>b</sup> School of Materials Science and Engineering, Southwest Jiaotong University, Chengdu, Sichuan, 610031, China

<sup>c</sup> Reactor Engineering Research Sub-institute, Nuclear Power Institute of China, Chengdu, 610005, China

<sup>d</sup> School of Engineering and Materials Science, Queen Mary University of London, London, E1 4NS, United Kingdom

<sup>e</sup> Institute for Applied Materials (IAM-WK), Karlsruhe Institute of Technology (KIT), Karlsruhe, 76131, Germany

## ARTICLE INFO

### Keywords:

High entropy alloy  
Laminated structure  
Graphene film  
Strength-plasticity synergy  
Strengthening mechanism

## ABSTRACT

Inspired by the design principle of pearl structure, a bottom-up flake powder self-assembly arrangement strategy, flake powder metallurgy, is used to prepare graphene films (GFs) reinforced CoCrFeNiMn high-entropy alloy (HEA) matrix composites with a pearl laminated structure. Flaky HEA powder was prepared by ball milling method and homogeneously mixed with Ni plated GFs. Vacuum hot-press sintering (VHPS) technique was carried out to solidify the mixed powders to obtain composites with uniform distribution of GFs(Ni) and flaky HEA. The results show that the bottom-up preparation strategy can effectively fabricate bionic laminated HEA matrix composites, and the composites have a distinct pearly laminated structure. The tensile strength of the composites with 5 vol% GFs(Ni) content reached 834.04 MPa, and the elongation reached 26.58 %. The compressive strength in parallel and perpendicular laminar directions reached 2069.66 MPa and 2418.45 MPa at 50 % strain, respectively. The laminated GFs(Ni)/HEA matrix composites possessed excellent strength and maintained good plasticity. In this study, the strengthening and toughening mechanism of the laminated GFs(Ni)/HEA matrix composites is discussed in detail, and the results show that the laminated structure and GFs(Ni) are favorable for the hardening and strengthening of the HEA matrix.

## 1. Introduction

The more common definition of HEA is currently defined as one those consisting of more than four body elements, each with a content of between 5 at.% and 35 at.%, generally forming a high-entropy solid solution [1–3]. At the earlier stage of exploration, HEA was mostly composed of components with iso-atomic ratio. The multiplicity of components in HEA results in a high entropy of mixing. The higher mixing entropy inhibits the formation of intermetallic compounds, which leads to the formation of multi-component mixed phases, resulting in a simple solid solution structure [4,5]. HEA complements each other through the interaction of its constituent components to achieve superior performance beyond that of a single component alloy.

By virtue of its multi-component nature, HEA exhibits synergistic effects of multiple strengthening mechanisms (including fine grain strengthening, solid solution strengthening, dislocation and twin strengthening, etc.) during the deformation process [6–8]. HEAs improve on traditional alloys with superior mechanical properties such as high fracture toughness, high hardness and strength, and excellent thermal stability [9–11]. The mechanical properties of HEAs are closely related to the composition, phase structure. Face-centered cubic (FCC) HEAs have better toughness but are softer [12], while body-centered cubic (BCC) HEAs have higher hardness and brittleness [13].

Due to the contradiction between strength and toughness, how to develop high-entropy alloy-based materials that jointly possess excellent strength and plasticity is one of the main issues at present [14].

\* Corresponding author. Key Laboratory of Advanced Technologies of Materials, Ministry of Education, Chengdu, 610031, China.

\*\* Corresponding author. Reactor Engineering Research Sub-institute, Nuclear Power Institute of China, Chengdu, 610005, China.

E-mail addresses: [xsjiang@swjtu.edu.cn](mailto:xsjiang@swjtu.edu.cn) (X. Jiang), [rexroi@hotmail.com](mailto:rexroi@hotmail.com) (T. Liu).

According to the Hall-Petch relationship, grain refinement can strengthen alloys without changing the composition. Simply by grain refinement, the strength of alloys will be effectively enhanced, but the plasticity is usually affected. For the synergy of strength and plasticity, in recent years it is common to improve it by structural design. Commonly, there are non-homogeneous structures such as pearly laminar structure, harmonic structures, bimodal structures, etc. [15,16]. The pearl laminate is a micro-scale laminate biomimetic structure that offers great advantages in maintaining strength and plasticity [17]. Lamellar structure deflects cracks to dissipate more energy during crack extension for plasticity and toughness increase, and lamellar structure also affects the arrangement of reinforcement for load transfer by reinforcement [18]. In graphene reinforced metal composite systems, the design of nanocarbon/laminar structures has been increasingly investigated [19]. Incorporating graphene reinforcement into the laminate structure will result in a high-density interface, which is capable of increasing the strength and maintaining good plasticity of the composites [20].

The graphene films (GFs) are a new type of 2D carbon nanomaterials. GFs are made of multilayer graphene stacks, retaining the desirable properties of single-layer graphene [21]. GFs have superb mechanical, electrical and thermal properties, thus gradually becoming a new direction to explore in the field of composites [22,23]. In the system of nano-carbon/CoCrFeNiMn HEA matrix composites, there are several major problems: 1) The interfacial bonding between graphene and HEA matrix is not easy, due to the large free energy of graphene's own surface and its large differences in structure and properties with HEA-based [24]. 2) GFs are prone to agglomeration by van der Waals forces, which can easily form defects and stress concentrations in the composites, which can affect the mechanical properties of the composites [25]. 3) The low entropy of the mixing of C and Cr elements leads to a severe interfacial reaction, which hinders the normal action of GFs in the HEA matrix. X.N. Mu et al. [26] fabricated titanium matrix composites with multilayer graphene (MLG) by flake powder metallurgy technology. Compared with monolithic pure Ti (HR normal), MLG-reinforced laminate composites showed 280 % (~2 GPa) increase in yield strength, substantially higher hardness, and increased plasticity. Common dispersion methods include molecular-level mixing [27], in situ growth [28], intense plastic deformation [29], and ball milling [30], etc. Among them, ball milling dispersion is considered to be a relatively simple and efficient method. The GFs were pre-treated with chemical plating to prepare a dense Ni coating on the surface. Thus, the bonding problem between GFs and HEA matrix with interfacial reaction can be solved.

In this study, a bottom-up flake powder self-assembly method was used to prepare HEA matrix composites with laminated structures, i.e., flake powder metallurgy. In this study, GFs (Ni) with uniform metallic Ni coating were prepared using chemical plating. Spherical HEA powder was broken into flakes by ball milling and homogeneously mixed with GFs(Ni). GFs(Ni)/HEA-based composites with pearl laminar structure were successfully prepared using vacuum hot press sintering (VHPS). In order to explore the effects of the lamellar structure and GFs(Ni) on the composites, the microstructure was analyzed using XED, SEM, EDS and TEM tests, and tensile experiments and compression experiments in different directions were performed. The results of mechanical property tests show that the laminated GFs(Ni)/HEA matrix composites have excellent tensile strength and maintain good plasticity. The results of microstructure analysis show that the laminated GFs(Ni)/HEA matrix composites have various strengthening mechanisms (solid solution strengthening, second phase strengthening, dislocation and twin strengthening, etc.). The results of microstructure analysis show that the laminated GFs(Ni)/HEA matrix composites have excellent tensile strength and maintain good plasticity.

## 2. Materials and methods

### 2.1. Raw material

GFs were used as the reinforcement material (density of 1.85 g/cm<sup>3</sup>, thickness of 0.012 mm). The matrix material was pre-alloyed CoCrFeNiMn high-entropy alloy powder (particle size 45–105 μm) with equal atomic ratio. The process parameters of mechanical ball milling for the preparation of flaky HEA powders were determined through preliminary pre-experiments. The HEA powder was first ball-milled in a carbide jar for 11 h, followed by the addition of GFs and mixing for 1 h. The ball-milling process used tert-butanol as a spacer protection medium, and the rotational speed was 300 rpm/min throughout the ball-milling process. Subsequently, vacuum freeze-drying was performed for 24 h to remove the protective medium tert-butanol to obtain a homogeneous mixed powder of GFs with flaky HEA.

The preparation of Ni coatings on the surface of GFs was adopted as chemical reaction depositions. First, the GFs were roughened in ethanol hydrochloric acid solution. Sensitization and activation treatment processes are required before preparing Ni coatings on GFs. The sensitization solution was made of SnCl<sub>2</sub> mixed with HCl. The activation solution consisted of PdCl<sub>2</sub> mixed with HCl. The main salt component was composed of NiSO<sub>4</sub>·6H<sub>2</sub>O, CH<sub>6</sub>NaO<sub>37</sub>, NH<sub>4</sub>Cl, and NaH<sub>2</sub>PO<sub>2</sub>. The pH of the solution was controlled between 9 and 10 using ammonia speaking solution. The nickel-plating times for the GFs were chosen to be 10, 20 and 30 min, respectively. After the nickel plating was completed, the GFs were dried at 90 °C for 5 h to obtain the GFs uniformly coated by nickel.

Finally, nickel-plated GFs strongly toughened laminated CoCrFeNiMn high-entropy alloy matrix composites were fabricated via VHPS. The temperature was increased to 1000 °C at a rate of 10 °C/min and gradually pressurized to 30 MPa, held for 1 h and then cooled with the furnace. The process flow diagram of the fabricate is shown in Fig. 1.

### 2.2. Characterization of composites

The nickel-plated GFs were subjected to microscopic morphology observation by scanning electron microscope (SEM, ZEISS Gemini 300) to obtain the optimal experimental parameters for nickel plating. After the sintered blocks were cut out to a specific size by wire cutting, their morphology was initially observed by optical microscopy (OM, Zeiss AXIO), followed by the characterization of the microscopic constituents using X-ray Diffraction (XRD, Rigaku Ultima IV) and SEM to characterize the organization of the microstructure of the composites. In addition, the 5 vol% GFs(Ni)/HEA matrix composites were further analyzed by transmission electron microscopy (TEM, FEI Tecnai F30) for microstructure analysis, selected area electron diffraction (SAED) for determining the tissue composition of the second phase, and high-resolution transmission electron microscopy (HRTEM) for analyzing the microstructure and interfacial bonding between the matrix and the second phase.

### 2.3. Mechanical performance tests

The drainage method was utilized to measure the density of the wire-cut blocks. From this, the densities of the sintered samples were further calculated. The hardness of the composites was tested utilizing a microhardness tester (HVS-1000Z) (load of 1000 gf, loading time maintained at 15s). The test samples are measured at five positions in a specific order of arrangement, thus avoiding errors caused by the specificity of the test positions. Subsequently, their mechanical properties in tension and compression were measured using a universal testing machine (WDW-3100). The tensile samples were tested using horizontally oriented (perpendicular to the laminar direction) I-beams with four tests in each group to minimize errors. The microstructure and fracture morphology of the tensile fracture were characterized and

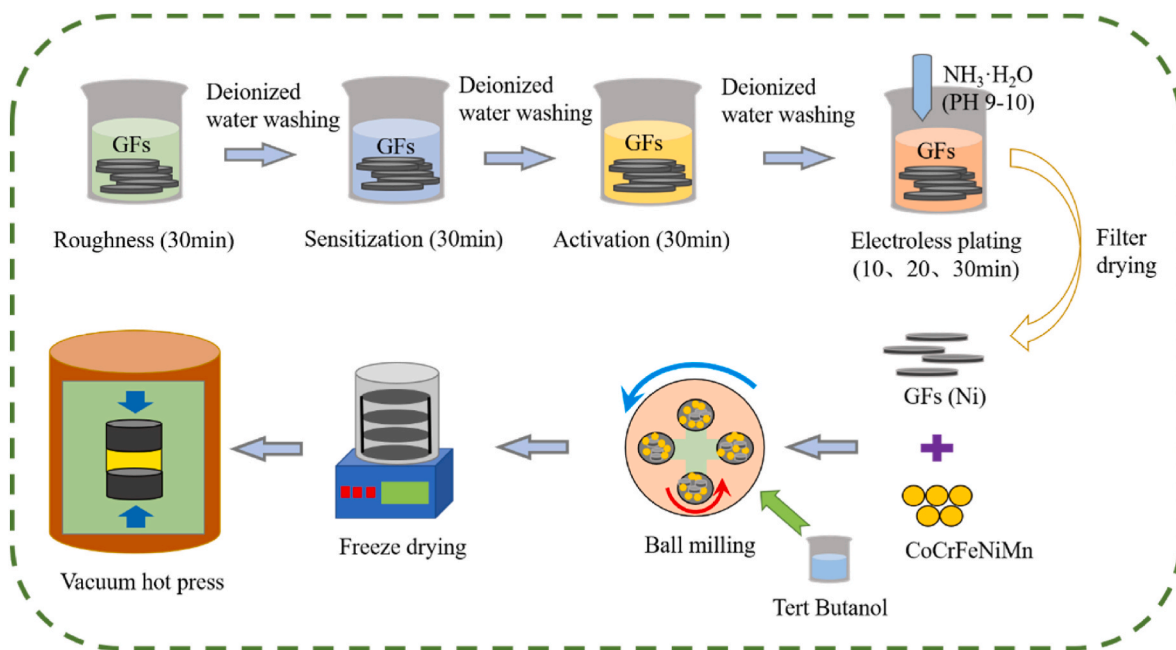


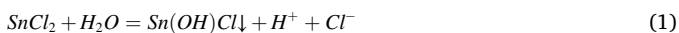
Fig. 1. Schematic diagram of the preparation process of laminated GFs(Ni)/HEA matrix composites.

analyzed using SEM. The compression experiments were conducted along the laminar direction and perpendicular to the laminar direction, and each group was also tested four times.

### 3. Results and discussion

#### 3.1. The formation mechanisms of GFs(Ni)

Through the chemical plating process, the nickel element can form a uniform and suitable thickness of cladding layer on the surface of the GFs. The surface of the GFs is roughened by ultrasonic cleaning and magnetic stirring. During the sensitization of the GFs in stannous chloride solution, the following hydrolysis reactions of stannous chloride occur [31,32] :

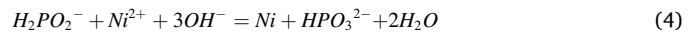


During the sensitization procedure,  $\text{Sn}^{2+}$  was distributed relatively uniformly on the morphology of the GFs surface without obvious preferential attachment. In order to facilitate the subsequent activation process,  $\text{Sn}^{2+}$  could fully react with  $\text{Pd}^{2+}$  to generate Pd element. It was necessary to inhibit the hydrolysis reaction of  $\text{Sn}(\text{OH})\text{Cl}$  as shown in Eq. (1). Therefore, it is necessary to add HCl content to the sensitization process. Following the activation of the GFs in palladium chloride solution, for ensuring a sufficiently high level of  $\text{Sn}^{2+}$  for the reduction of elemental Pd. It was necessary to inhibit the oxidation reaction of  $\text{Sn}^{2+}$  to generate  $\text{Sn}^{4+}$  as shown in Eq. (3), and thus the concentration of concentrated hydrochloric acid was reduced in the activation solution to lower the concentration of  $\text{H}^+$  in the solution [33] :



In the process of activation, Pd element has two tendencies. One tends to be enriched at the edges or folds of GFs, whose surface-active functional groups can promote the growth of Pd element; the other tends to react with  $\text{Sn}^{2+}$  at  $\text{Sn}^{2+}$  to generate Pd element. Finally, during the formation of the nickel plating layer,  $\text{Ni}^{2+}$  is reduced to generate Ni attached to the surface of GFs with Pd element as the autocatalytic active center. In the plating solution, nickel sulfate hexahydrate, as the main

source of  $\text{Ni}^{2+}$ , reacts with  $\text{H}_2\text{PO}_2^-$  under alkaline conditions to generate Ni by redox reaction, as shown in Eq. (4), and finally forms a metallic nickel particle cladding layer on the surface of GFs.



Different chemical plating time has different effects on the metal plating layer, so the pre-experiment of 0–30 min was carried out respectively, as shown in Fig. 2. It is obvious that after 10 min of magnetic stirring, the nickel film is not well-deposited on the GFs and the thickness of the deposition is thin due to the insufficient reaction caused by the short time. After 20 min of magnetic stirring, the nickel film is uniformly deposited on the GFs and the plating layer gradually becomes thicker. After 30 min of magnetic stirring, with the continuous consumption of the reactants, the plating concentration of the solution will gradually decrease, and the deposition rate of nickel layer will also decrease, when the deposition speed is also decreased. When the deposition speed is less than the magnetic stirring peeling speed, so there is a nickel layer peeling off the nickel layer, resulting in an uneven phenomenon of the nickel layer. Therefore, 20 min was chosen as the optimum plating time.

#### 3.2. Microstructure characterization

Fig. 3 presents the XRD images of laminated high-entropy alloy matrix composites with diverse GFs contents. The XRD results show that there are two distinct phases in the composites, and the matrix is a simple FCC structure of CoCrFeNiMn high-entropy alloy, which corresponds to the (111), (200), (220), respectively. The phase of the CoCrFeNiMn HEA was not changed by the addition of GFs. As the content of GFs increases, the diffraction peaks of the  $\text{Cr}_7\text{C}_3$  phase increase. It is due to high temperature and high pressure sintering that Cr reacts with C very easily, leading to the formation of carbides, and thus the  $\text{Cr}_7\text{C}_3$  phase appears. N.D. Stepanov et al. [34] revealed that the element Cr is the strongest metal carbide forming element in the CoCrFeNiMn HEA system, and the appearance of the  $\text{Cr}_7\text{C}_3$  phase was also found in the study, thus confirming that the element Cr is the strongest metal carbide forming element in this HEA. Similarly, H. Xu et al. [35] research on graphene-coated CoCrFeMnNi high-entropy alloy matrix composites found that the  $\text{Cr}_7\text{C}_3$  phase also appeared with increasing time of ball

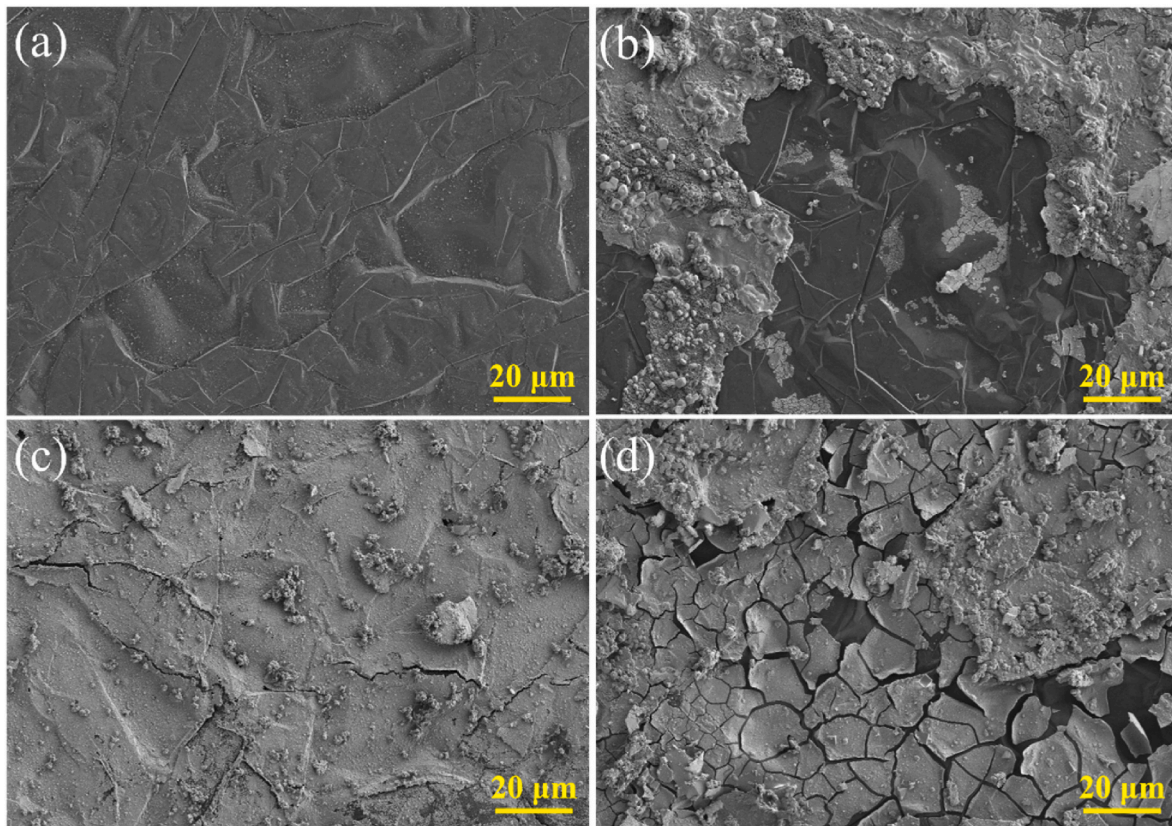


Fig. 2. SEM images of GFs at different nickel-plated times: (a–d) 0, 10, 20, 30min.

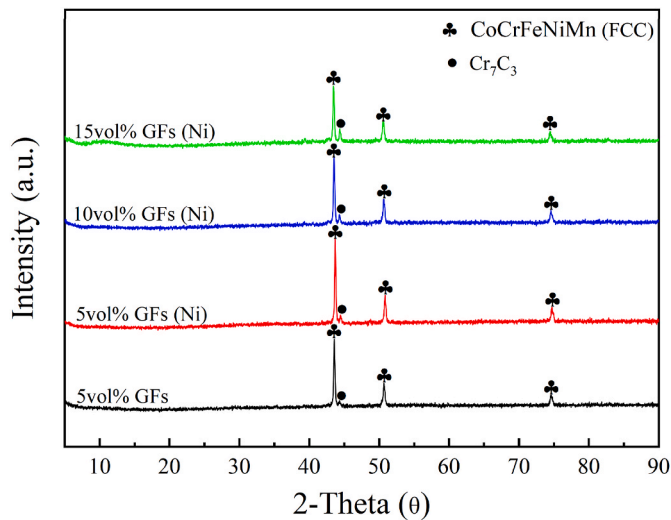


Fig. 3. XRD images of laminated GFs(Ni)/HEA matrix composites with different GFs contents.

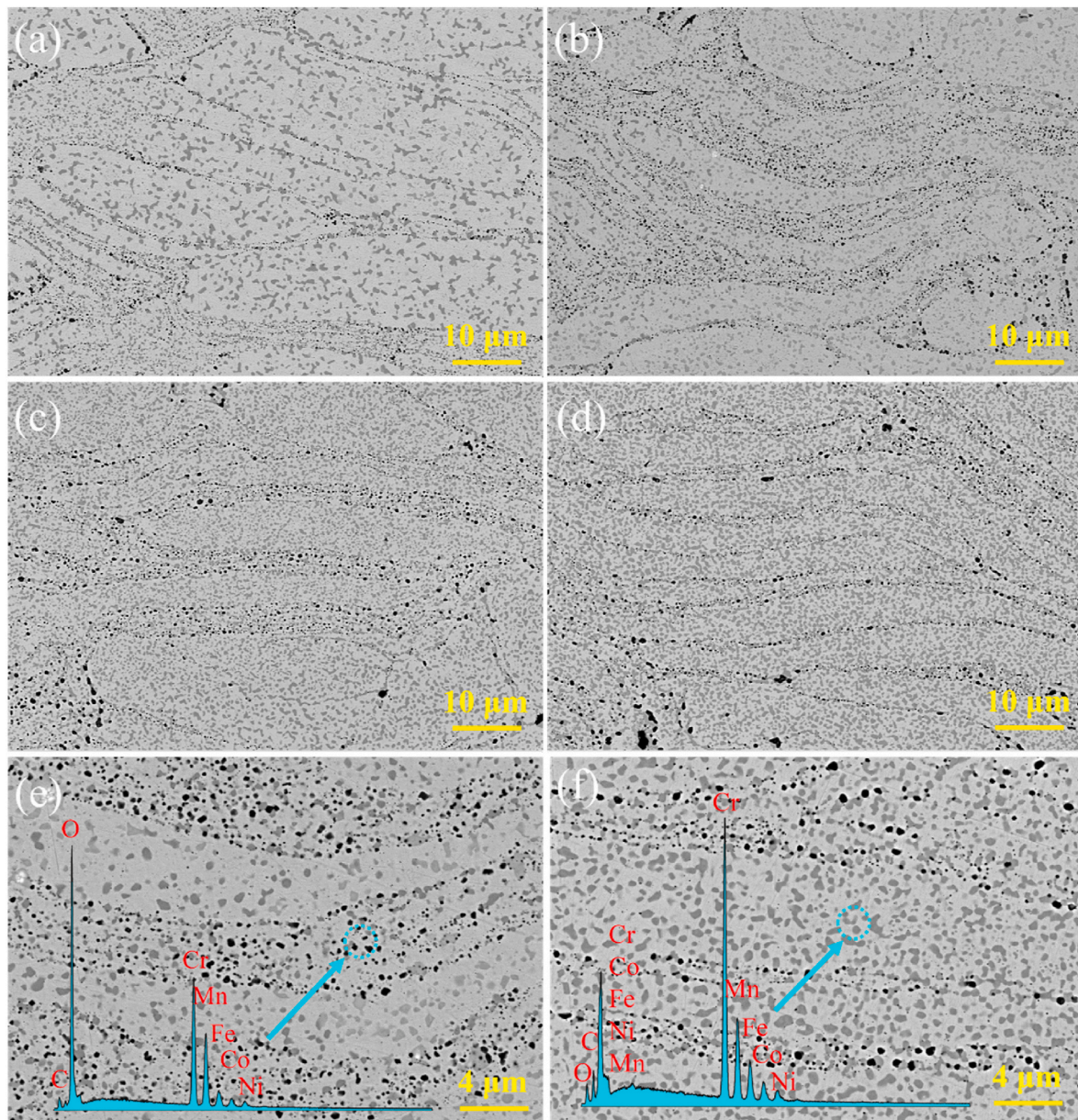
milling.

Fig. 4 shows the SEM image of the block cross-section of the composites after sintering. The microstructure of the composites has obvious laminar organization (As shown in Fig. 4). The flaky CoCrFeNiMn HEA particles constitute “bricks”, and the crushed HEA powder constitutes “mortar”, which together constitute the pearl laminar structure. The flaky HEA powder will be aligned in sequence under the action of gravity, and gradually converge to the same, so the flaky powder metallurgy method can be a better preparation of composites with laminar structure. The white phase is the matrix phase of CoCrFeNiMn HEA in

the composites, and the gray phase and black phase are the second phase generated after sintering. The gray phase is uniformly distributed between the composites and its amount is affected by the content of GFs. The black phase is concentrated between the “brick” layers. Fig. 4 (e, f) shows the energy spectrum analysis of the black phase and gray phase in the composites, respectively. The black phase is an oxidized phase, which gathers at the broken particles between the flaky HEA powders, indicating that oxygen was mixed in during the ball milling process and combined with the crushed HEA particles. The gray phase is a carbonized phase and is uniformly distributed with the composites. This is due to the enhancement of atomic diffusion ability during the sintering process in the high temperature environment of the sintering process, which causes the intensification of the diffusion and reaction between Cr and C elements, resulting in the formation of the carbonized phase.

### 3.3. Microstructure characterization by TEM

In order to further characterize the microstructure in the laminated GFs(Ni)/HEA matrix composites, TEM was characterized on the 5 vol% GFs(Ni)/HEA matrix composites. Fig. 5 shows the TEM elemental distribution images of the microstructure in the laminated GFs(Ni)/HEA matrix composites. Co, Fe, and Ni elements are homogeneously distributed in the composites, and Cr, Mn, O, and C elements are locally aggregated in the composites. The distribution of Cr, Mn, O, and C elements has a certain pattern. The similarity of the distribution areas of Cr and C elements indicates that a chemical reaction has occurred between Cr and C. The sintering process led to the enhancement of the diffusion capacity of the elements. The C element to fully diffuse and synthesize the second phase with Cr. The similar distribution of Mn and O elements indicates that the O element combines with Mn, which is caused by the mixing of oxygen in the experimental process. The full diffusion of the elements after vacuum hot-pressing sintering also led to the full combination of Mn and O to produce another second phase.



**Fig. 4.** SEM images of the GFs/HEA matrix composites: (a) 5 vol% GFs; (b–d) 5, 10, 15 vol% GFs (Ni); (e) (f) energy spectra of oxide and carbide phases, respectively.

Fig. 6 shows the TEM images of the microstructure of the laminated GFs(Ni)/HEA matrix composites. As shown in Fig. 6(a), the microstructure of the composite mainly consists of the matrix phase, the oxide phase and the carbide phase, which is the same as the results in Fig. 5. As can be seen in Fig. 6(b), a large number of dislocations and twin crystals exist in the composite. Numerous dislocations are distributed around the twin, which indicates that there is a certain connection between the twin crystals and the generation of dislocations. Fig. 6(c, e) and (d, f) show the diffraction patterns and the HRTEM of the twin crystals and the matrix, respectively, and it is known that the lattice spacing of both the twin crystals and the matrix is 0.204 nm by Fast Fourier Transform (FFT) of the HRTEM. The presence of numerous dislocations and lattice aberrations in the matrix is found through the FFT of the matrix. Because of the different coefficients of thermal expansion of the matrix and the second phase. Their deformation disparity produces thermal mismatch stresses and lattice distortions during temperature changes, resulting in massive dislocations. The presence of a large number of defects and lattice distortions at the grain boundaries leads to a high distortion energy at the grain boundaries. When dislocations move to the grain

boundaries, they are hindered and entanglement and plugging occurs. CoCrFeNiMn high-entropy alloy mainly focuses on the dislocation slip at the initial deformation stage, and the dislocations are hindered when they are moved to the grain boundary or the second-phase particles. After numerous dislocations are hindered, the deformation induces twinning, with stacked layer dislocations as the core of the deformation twinning nuclei [36]. The creation of the second phase increases the density of the phase boundary, creating an additional obstacle for dislocation slip and thus promoting strain hardening. The continuous generation and entanglement of dislocations and the continuous formation of new twins lead to an increasing interface density. Consequently, the composites contribute significantly to the synergy of plasticity and strength through multiple deformation mechanisms (i.e., dislocation slip, entanglement, twinning, etc.). In addition, the composites have improved strength through solid solution strengthening and increased interfacial density. Plasticity is enhanced by dislocation shifts, phase transitions, etc. [37].

Due to the existence of two different second phases in the composites, the bonding of the 2 s phases to the matrix are unknown. Therefore,

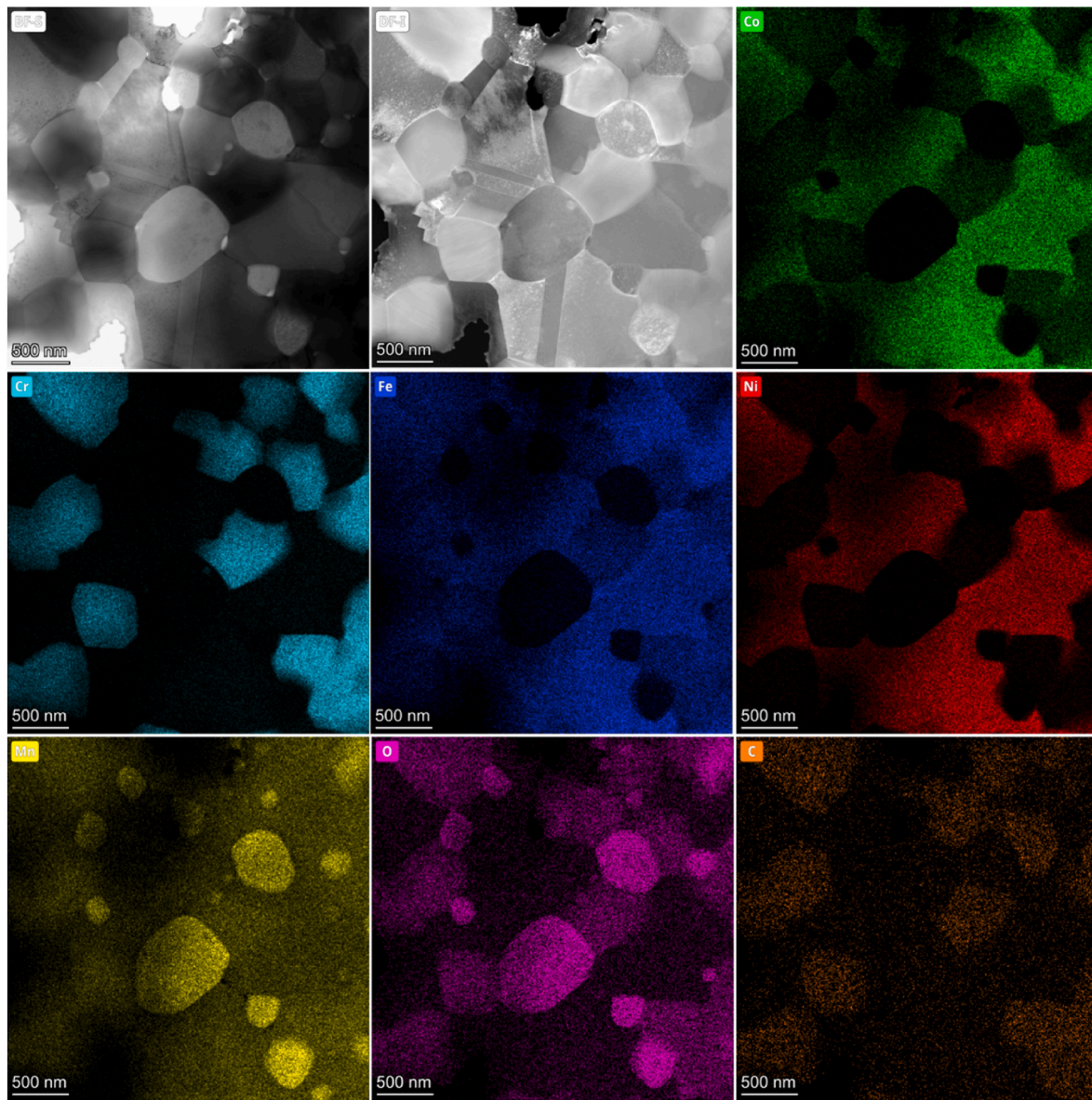


Fig. 5. TEM elemental distribution images of laminated GFs(Ni)/HEA matrix composites.

further HRTEM characterization was performed separately. Fig. 7(a, b, e) and (c, d, f) show the TEM images and diffraction patterns of the contact interface between the oxide phase, the carbide phase and the matrix. According to the results of the diffraction pattern, it can be seen that the oxidized phase is  $Mn_2O_7$ , and the lattice spacing  $d$  is 0.496 nm, while the carbonized phase is  $Cr_7C_3$ , and the lattice spacing is 0.605 nm, which coincides with the results of XRD and EDS. In the HRTEM images of the oxide and carbide phases, it can be seen that the oxidized and carbonized phases are well bonded at the interface with the matrix and are in direct contact at the atomic scale. The mixing enthalpies of the Fe–Co–Ni–Cr–Mn and C are negative, which facilitates the bonding with C during the sintering process. Among them, Cr has a low enthalpy of mixing with C and has a particularly strong binding force, so that Cr reacts with C very easily. The HEA particles produce a large number of broken particles during mechanical ball milling with residual air, so that O undergoes an oxidation reaction with the Mn element. In addition, due to the high-temperature and high-pressure environment of the sintering process, although it makes the composite material obtain high densification after powder metallurgy. The high-temperature environment also makes the diffusion ability of each element increase, which makes the

intensification of elemental segregation, and finally leads to the formation of oxide phase and carbide phase. Therefore, the laminated GFs (Ni)/HEA matrix composites mainly composed of three phases (FCC solid solution in the matrix,  $Mn_2O_7$  oxide phase, and  $Cr_7C_3$  carbide phase).

### 3.4. Mechanical properties

The density, hardness, tensile and compressive properties of laminated GFs(Ni)/HEA matrix composites are shown in Fig. 8. High densification is an important parameter for composites to have good properties. Hardness is also an essential parameter to indicate the softness or hardness of the composites. Density and hardness are also necessary parameters to measure the mechanical properties at present. From Fig. 8(a), it can be clearly concluded that the densities of the composites with different GFs contents are all above 95 %, presenting the high densities. Higher temperatures and higher loads are maintained during the vacuum hot press sintering process, which leads to further densification of the composites. The high densification ensures that there are fewer voids or micropores in the composites, which results in



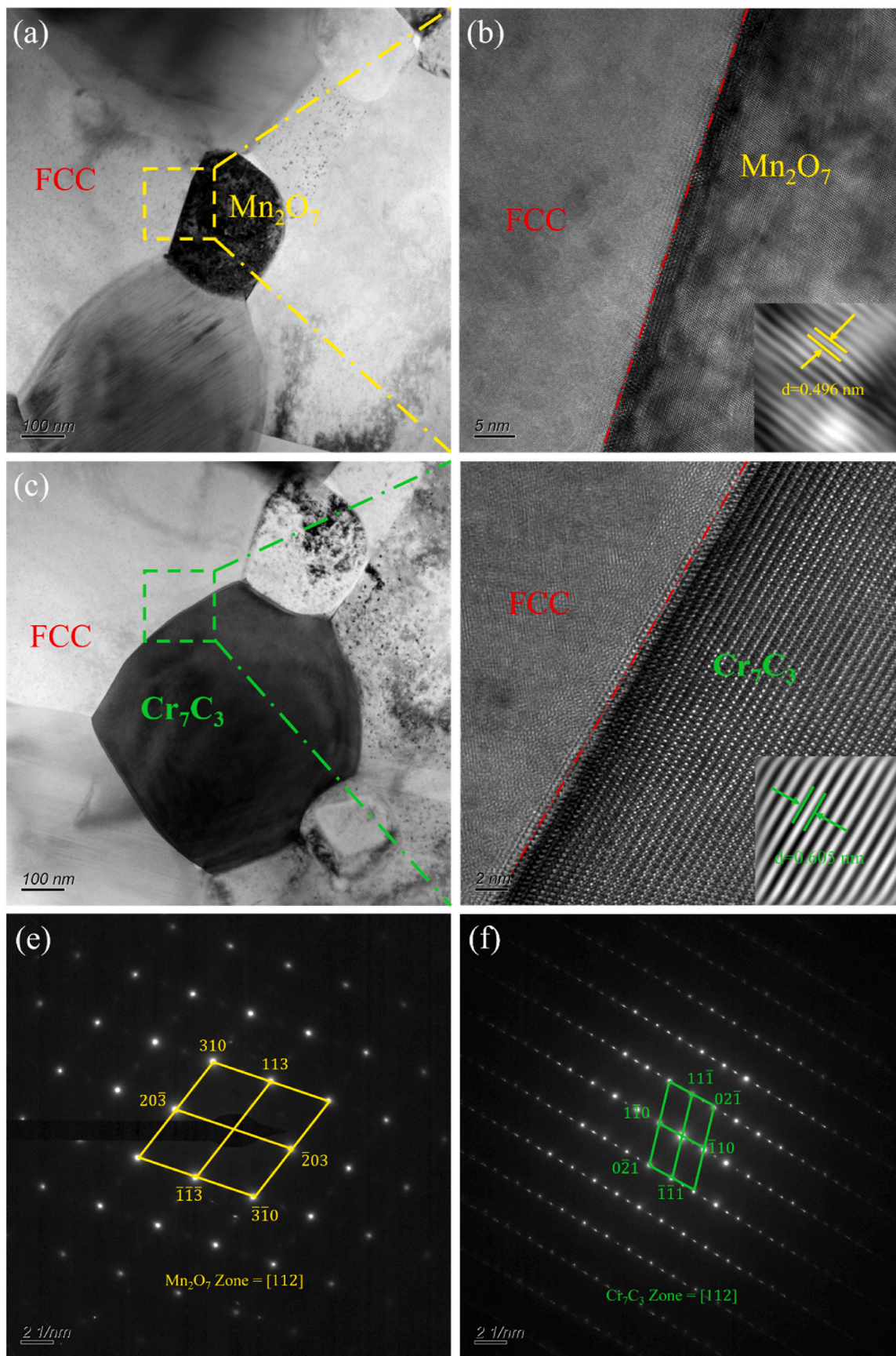
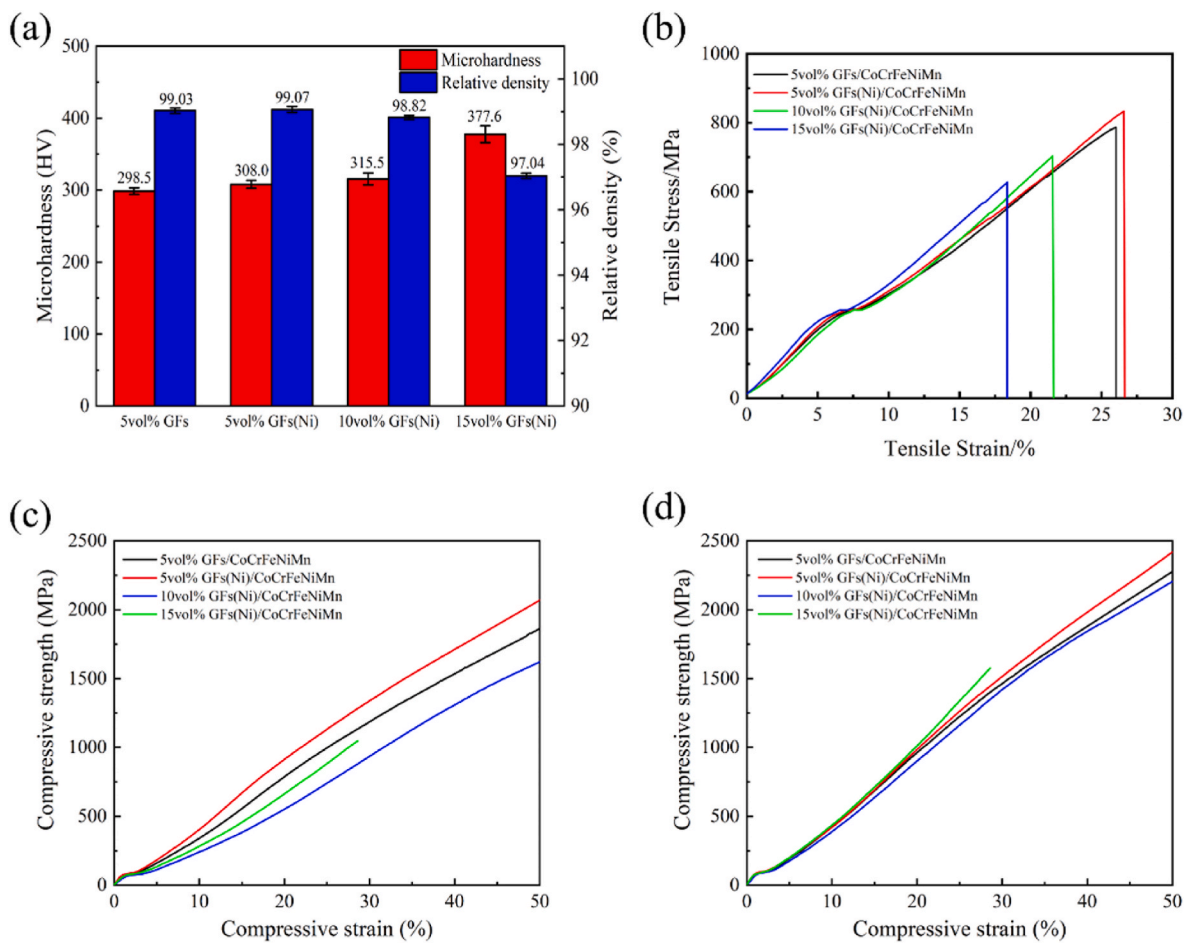


Fig. 7. TEM and HRTEM images of the oxide and carbide phases of the laminated GFs(Ni)/HEA matrix composites: (a, b) TEM of the oxides and the HRTEM images with respect to the matrix; (c, d) TEM of the carbides and the HRTEM images with respect to the matrix; (e, f) Diffraction patterns of the oxides and carbides.



**Fig. 8.** Images of mechanical properties of laminated GFs(Ni)/HEA matrix composites: (a) densities and hardness; (b) tensile curves; (c) compression curves in parallel laminate direction; (d) compression curves in perpendicular laminate direction.

fewer sources of crack initiation during plastic deformation and excellent mechanical properties. 15 vol% GFs content of the composites shows a slightly larger difference in densification than the other composites. This is due to the increase in GFs, agglomeration phenomenon occurs, which leads to the formation of micropores locally. 5 vol% GFs/HEA The hardness of the 5, 10, 15 vol% GFs(Ni)/HEA matrix composites were 298.5, 308.0, 315.5, 377.6 HV, respectively. Vickers hardness showed an increasing trend with the increase of GFs content. As shown in Fig. 8(b), the tensile curves of the composites with different GFs contents all showed a yielding stage first, followed by plastic deformation and finally fracture. The tensile strengths of 5 vol% GFs content of HEA, 5, 10, 15 vol% GFs(Ni) content of HEA matrix composites were 786.62 MPa, 834.04 MPa, and 703.41 MPa, respectively. And the post-break elongation was 25.95 %, 26.58 %, 21.56 %, and 18.3 %, respectively. The difference in strength of composites is due to two factors. On the one hand, due to the increase of reinforcing phase content, which leads to more second phase strengthening. On the other hand, it is due to the greater strength of graphene itself. The GFs content leads to the elevated strength of the composite [38].

Due to the anisotropy of the laminated structure, the properties of the laminated structure in different directions differ greatly. Compression experiments were carried out on different directions of the laminated structure to verify that the laminated structure can have the synergistic effect of strength-plasticity in the parallel laminar direction. Fig. 9(c and d) shows the compression curves in parallel and perpendicular laminate directions, respectively. When the content of GFs is low, the composites possess good plasticity. This resulted in the compression experiments not easily destroying the samples, so only

compression curves with 50 % of compressive strain were taken. The compressive strengths in the parallel laminar direction are 1864.12 MPa, 2069.66 MPa, 1622.01 MPa, 1047.14 MPa, respectively. The compressive strengths in the perpendicular laminar direction are 2276.34 MPa, 2418.45 MPa, 2205.28 MPa and 1577.64 MPa, respectively. The laminate structure can obtain a better strength-plasticity synergy, while the appropriate incorporation of GFs can effectively enhance the strength of the composites. For the same material, under the same stress conditions, when the bearing area is larger, its bearing capacity is stronger. Therefore, when the pressure perpendicular to the GFs bearing capacity should be stronger than parallel to the direction of the GFs, so that its compression strength is relatively large. The large difference in compressive strength between parallel and perpendicular laminae indicates the anisotropy of the laminae. Q. Zhang et al. [39] also found anisotropy in the compressive properties of laminated aluminum matrix composites when studying their mechanical properties. A. Shaga et al. [40] conducted compression experiments on Al–Si–Mg/SiC laminated composites and found that the compressive strengths loaded in different directions were different. All these results verify the existence of anisotropy in materials with a laminated organization. When subjected to external forces, the anisotropy of the lamellar organization leads to different forces in different directions. Moreover, GFs are also internally distributed along parallel laminar directions, which concentrates greater loads and consumes more energy during both tensile and compressive processes. Therefore, the combined effect of the laminate structure and GFs leads to obtaining more excellent mechanical properties of laminated GFs(Ni)/HEA matrix composites.

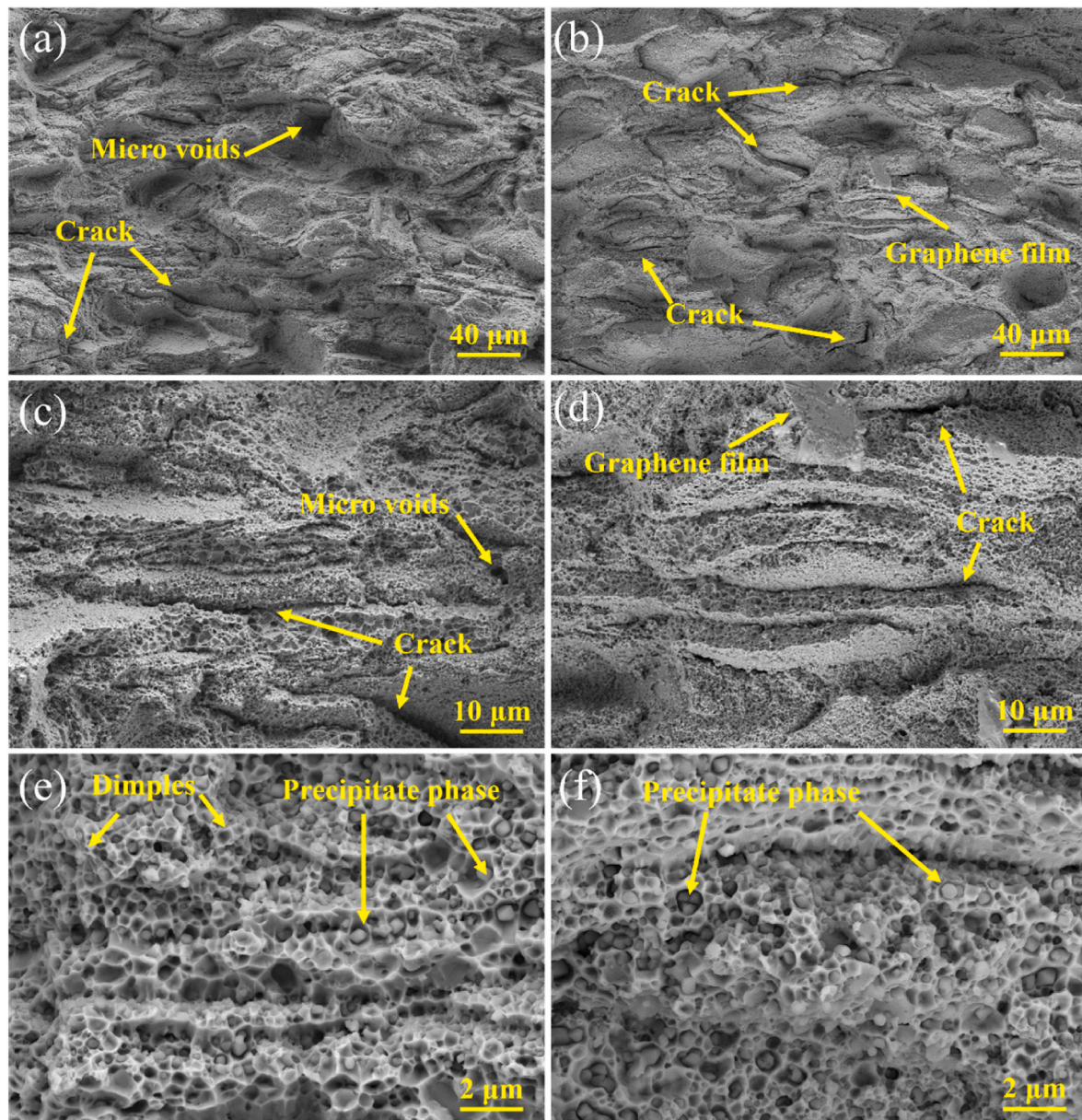


Fig. 9. SEM fracture morphology of tensile tests: (a, c, e) Laminated 5 vol% GFs/HEA matrix composites; (b, d, f) Laminated 5 vol% GFs(Ni)/HEA matrix composites.

### 3.5. Fracture behavior

SEM observations were carried out on the fracture morphology of the tensile test so as to analyze the strong toughening mechanism and fracture mechanism of the composites, the SEM images are shown in Fig. 9. Fig. 9 (a, c, e) and (b, d, f) are the tensile fracture morphology of GFs and GFs(Ni) composites with 5 vol% content, respectively. From the tensile fracture morphology images, it can be seen that both the laminated GFs/HEA and GFs(Ni)/HEA matrix composites exhibit a distinct laminated structure. The composites with GFs(Ni) showed a more pronounced laminated structure relative to the fracture phase appearance of the composites with uncoated GFs with nickel. It is obvious that the composites have a clear laminated structure as shown in the two figures of Fig. 9(a and b) at low magnification. The “brick” structure is composed of flaky HEA particles, while the GFs and broken particles are mixed to form a “mortar” structure.

In Fig. 9(c and d), numerous cracks in the fracture profile of the composite. These cracks are distributed in the “mortar” position and along the “brick” structure. Moreover, extracted GFs are found in the

tensile fracture, and it can be inferred that the laminated structure prevents the cracks from expanding and changes the direction of crack expansion. Fig. 9 (e, f) shows high magnification SEM images of the fracture morphology, which demonstrates extensive dimples. The presence of numerous dimples proves that the fracture of composites is a typical ductile fracture process. Second phase particles are present in the dimples is due to the dislocations moving to the second phase particles for entanglement and stacking during the tensile process. The different plasticity of the matrix and the second phase particles. When fracture occurs due to stress concentration up to the fracture strength, it leads to the creation of dimples around the stiffer second-phase particles.

### 3.6. Strengthening and toughening mechanism

On the basis of the SEM and TEM results images, the strengthening and toughening mechanism of the laminated GFs/HEA matrix composites was plotted, as shown in Fig. 10. During the loading process, microcracks gradually form and grow, and converge in the “mortar” layer. As the tensile process proceeds, the micro-cracks and micro-holes

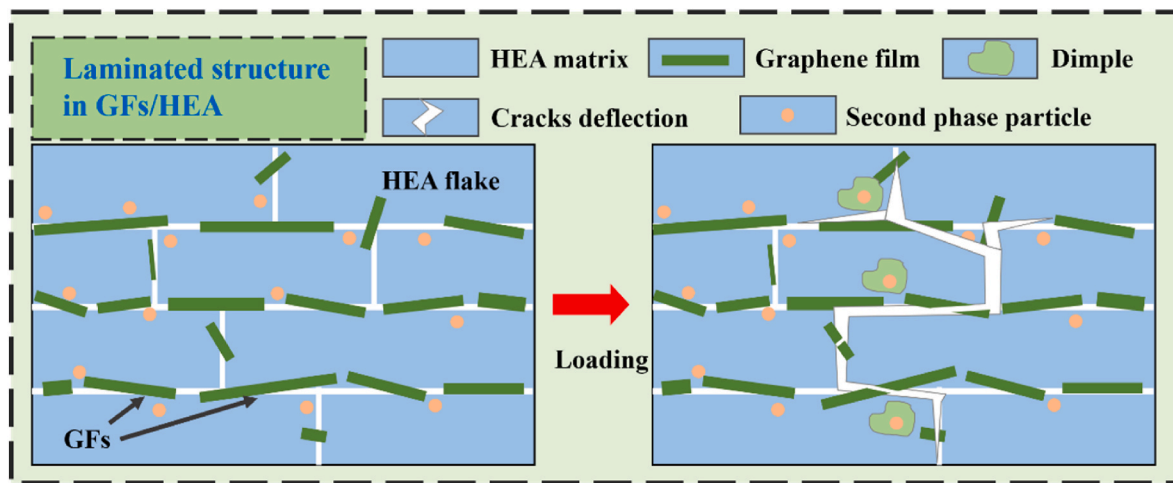


Fig. 10. Schematic diagram of strengthening and toughening mechanism of laminated GFs/HEA matrix composites.

gradually merge and expand to form cracks. Deflection of cracks due to the presence of the “pearl-like layer” of laminated structure [41]. C. Ferraro et al. [42] also studied  $\text{Al}_2\text{O}_3/\text{Al}$ -4 wt. %Mg layered composites and visualized crack deflection due to the layered structure by optical microscopy and electron scanning microscopy. Crack deflection will make the crack extension path become curved, and the energy consumed for crack extension into a curved path will be much more than that for linear extension, so the stress release from crack deflection will be more, which contributes to improve the composites plasticity and toughness [43,44].

A variety of strengthening mechanisms exist in the laminated GFs (Ni)/HEA matrix composites. The plastic deformation that occurs during ball milling of HEA powder results in a large amount of residual stress in the composite, which prevents the movement of dislocations and produces strain reinforcement. In addition, as can be seen from the TEM images in Fig. 5, the grains of the HEA matrix composites are small, almost all of them are in the nanometer scale. The fine grains lead to the increase of grain boundaries, which will hinder the dislocations from moving across the grains and plugging at the grain boundaries, resulting in fine grain strengthening. During the sintering process of GFs, part of the carbon element will solidly dissolve into the HEA matrix to conduct solid solution strengthening. The solid solution of C elements into the HEA matrix results in a certain degree of distortion of the crystal lattice, which generates a micro-area stress field near the distortion region. The micro-area stress field will hinder the dislocations and makes it difficult to move the dislocations, and thus improves the strength of the composites. The micro-structure of the composites consists of HEA matrix, carbide phase and oxide phase. The appearance of the second phase particles (carbide and oxide phases) similarly impedes the dislocation motion and produces second phase strengthening. When the dislocations encounter the carbide and oxide phase, the second-phase particles will cause some obstruction to the movement of dislocations, making the dislocation movement difficult. Therefore, the strength of composites is further increased by the second phase reinforcement. The reinforcing phase has an effective load transfer, which is also one of the ways of effective reinforcement. Among them, good interfacial bonding is the guarantee of effective load transfer. L. Meng et al. [45] prepared graphene nano-sheets magnesium matrix composites, which have good interfacial bonding, resulting in composites with better reinforcement than other magnesium matrix composites.

Differences in the thermal expansion coefficients of the GFs and the HEA matrix lead to thermal mismatch strengthening. Thermal mismatch generates localized residual stresses between the reinforcement and matrix, which causes an increase in dislocation density. The increase in dislocation density makes the dislocations more susceptible to entan-

glement and impedes the movement of the dislocations, which further strengthens the composite [46]. L. Shen et al. [46] similarly found thermal mismatch strengthening of the reinforcing phase with the matrix in their experiment via the analysis of the reinforcement mechanism of FeCrNiCo HEAs by micrometer TiC and nano-SiC particles. According to W.S. Miller et al. [47] the following equation was proposed:

$$\sigma_d = \alpha G b \rho^{\frac{1}{2}} \quad (5)$$

$$\rho = \frac{1.2 \Delta T \Delta C F_v}{b d} \quad (6)$$

where  $\alpha$  is the dislocation enhancement factor,  $G$  is the shear modulus,  $b$  is the Burgner vector,  $\rho$  is the dislocation density,  $\Delta T$  is the temperature change,  $\Delta C$  is the coefficients of thermal expansion,  $d$  is the reinforcement size and  $F_v$  is the volume fraction. Combined with Eq. (5) and (6), it is further revealed that the thermal expansion coefficients of GFs are different from those of the HEA matrix, which leads to an increase in the dislocation density. This leads to an increase in residual stresses and dislocations, which improves the strength of the composite. Which improves the strength of the composite. Thereby, the strength of the composites is increased. Therefore, during the process of tensile fracture, due to the presence of different second-phase particles in the composite, which will lead to localized inhomogeneities in the deformation. As the plastic deformation continues, micropores are formed in the most severely deformed regions (at the second phase particles). Under continuous external tensile loading, the micropores gradually expand and merge to form holes. The holes begin to grow and accumulate, eventually forming cracks and leading to failure of the composite.

#### 4. Conclusion

In this study, GFs(Ni)/HEA matrix composites with laminated structure were fabricated successfully by using flake powder metallurgy technique with VHPS method. The composites possessed excellent strength-plasticity synergy. The main conclusions are as follows.

- (1) The composites showed a unique “brick-mortar” pearly structure. The flaky HEA particles constitute the “brick” structure, while the GFs and the crushed HEA particles constitute the “mortar” structure. The strength-plasticity synergy is realized by the reinforcement of GFs and the laminated structure.
- (2) Optimal mechanical properties were obtained for 5 vol% GFs (Ni)/HEA matrix composites. The tensile strength reached 834.04 MPa with an elongation of 26.58 %. The compressive

strengths of parallel and perpendicular laminae at 50 % strain reached 2069.66 MPa and 2418.45 MPa, respectively. The composites possess excellent strength and maintain good plasticity.

- (3) The strengthening mechanism of composites is related to a variety of mechanisms (solid solution strengthening, fine grain strengthening, second phase strengthening, dislocation twinning, etc.). In addition, the laminate structure further strengthens the composite by deflecting and hindering the cracks by virtue of its anisotropy, maintaining its synergy of strength and plasticity.

#### Data availability statement

The data used to support the findings of this study are available from the corresponding author upon request.

#### Declaration of competing interest

The authors declare that they have no known competing financial interests or personal relationships that could have appeared to influence the work reported in this paper.

#### Acknowledgments

This work was supported by Key Laboratory of Infrared Imaging Materials and Detectors, Shanghai Institute of Technical Physics, Chinese Academy of Sciences (No. IIMDKFJJ-21-10) and China Postdoctoral Science Foundation (No. 2018T110993). We would like to thank Analytical and Testing Center of Southwest Jiaotong University for partial testing.

#### References

- Zhang H, Pan Y, He Y, Jiao H. Microstructure and properties of 6FeNiCoSiCrAlTi high-entropy alloy coating prepared by laser cladding. *Appl Surf Sci* 2011;257(6): 2259–63. <https://doi.org/10.1016/j.apsusc.2010.09.084>.
- Yeh JW. Alloy design strategies and future trends in high-entropy alloys. *Jom* 2013; 65(12):1759–71. <https://doi.org/10.1007/s11837-013-0761-6>.
- Senkov ON, Miller JD, Miracle DB, Woodward C. Accelerated exploration of multi-principal element alloys with solid solution phases. *Nat Commun* 2015;6(1). <https://doi.org/10.1038/ncomms7529>.
- Vikram RJ, Gupta K, Suwas S. Design of a new cobalt base nano-lamellar eutectic high entropy alloy. *Scripta Mater* 2021;202. <https://doi.org/10.1016/j.scriptamat.2021.113993>.
- Qiu X. Microstructure and mechanical properties of CoCrFeNiMo high-entropy alloy coatings. *J Mater Res Technol* 2020;9(3):5127–33. <https://doi.org/10.1016/j.jmrt.2020.03.029>.
- Tong YG, Tian N, Chen H, Zhang XC, Hu YL, Ji XX, et al. Real-time atomic deformation behavior of nano CoCrCuFeNi high-entropy alloy. *T Nonferrous Metal Soc* 2023;33(4):1156–63. <https://doi.org/10.1016/j.tsm.2023.03.011>.
- Zhang G, Liu H, Zheng K, Tang J, Shi Y, Cai B, et al. Effects of carbon doping on annealing behavior of a CoCrFeNiMn high-entropy alloy. *J Mater Res Technol* 2023;26:2711–23. <https://doi.org/10.1016/j.jmrt.2023.08.069>.
- Shahmir H, Mehranpour MS, Arsalan Shams SA, Langdon TG. Twenty years of the CoCrFeNiMn high-entropy alloy: achieving exceptional mechanical properties through microstructure engineering. *J Mater Res Technol* 2023;23:3362–423. <https://doi.org/10.1016/j.jmrt.2023.01.181>.
- Qiu J, Jin T, Xiao G, Wang Z, Liu E, Su B, et al. Effects of pre-compression on the hardness of CoCrFeNiMn high entropy alloy based an asymmetrical yield criterion. *J Alloys Compd* 2019;802:93–102. <https://doi.org/10.1016/j.jallcom.2019.06.159>.
- Wang AG, An XH, Gu J, Wang XG, Li LL, Li WL, et al. Effect of grain size on fatigue cracking at twin boundaries in a CoCrFeMnNi high-entropy alloy. *J Mater Sci Technol* 2020;39:1–6. <https://doi.org/10.1016/j.jmst.2019.09.010>.
- Yang L, Ge H, Zhang J, Xiong T, Jin Q, Zhou Y, et al. High He-ion irradiation resistance of CrMnFeCoNi high-entropy alloy revealed by comparison study with Ni and 304SS. *J Mater Sci Technol* 2019;35(3):300–5. <https://doi.org/10.1016/j.jmst.2018.09.050>.
- Chen LB, Wei R, Tang K, Zhang J, Jiang F, He L, et al. Heavy carbon alloyed FCC-structured high entropy alloy with excellent combination of strength and ductility. *Mater Sci Eng A-Struct* 2018;716:150–6. <https://doi.org/10.1016/j.msea.2018.01.045>.
- Ly S, Zu Y, Chen G, Zhao B, Fu X, Zhou W. A multiple nonmetallic atoms co-doped CrMoNbWTi refractory high-entropy alloy with ultra-high strength and hardness. *Mater Sci Eng A-Struct* 2020;795. <https://doi.org/10.1016/j.msea.2020.140035>.
- Ritchie RO. The conflicts between strength and toughness. *Nat Mater* 2011;10(11): 817–22. <https://doi.org/10.1038/nmat3115>.
- Koyama M, Zhang Z, Wang M, Ponge D, Raabe D, Tsuzaki K, et al. Bone-like crack resistance in hierarchical metastable nanolaminate steels. *Science* 2017;355(6329): 1055–7. <https://doi.org/10.1126/science.aal2766>.
- Lu K. Making strong nanomaterials ductile with gradients. *Science* 2014;345 (6203):1455–6. <https://doi.org/10.1126/science.1255940>.
- Espinosa HD, Juster AL, Latourte FJ, Loh OY, Gregoire D, Zavattieri PD. Tablet-level origin of toughening in abalone shells and translation to synthetic composite materials. *Nat Commun* 2011;2(1). <https://doi.org/10.1038/ncomms1172>.
- Huang W, Restrepo D, Jung JY, Su FY, Liu Z, Ritchie RO, et al. Multiscale toughening mechanisms in biological materials and bioinspired designs. *Adv Mater* 2019;31(43). <https://doi.org/10.1002/adma.201901561>.
- Si S, Li W, Zhao X, Han M, Yue Y, Wu W, et al. Significant radiation tolerance and moderate reduction in thermal transport of a thalsten nanofilm by inserting monolayer graphene. *Adv Mater* 2017;29(3). <https://doi.org/10.1002/adma.201604623>.
- Chen F, Ying J, Wang Y, Du S, Liu Z, Huang Q. Effects of graphene content on the microstructure and properties of copper matrix composites. *Carbon* 2016;96: 836–42. <https://doi.org/10.1016/j.carbon.2015.10.023>.
- Nieto A, Bisht A, Lahiri D, Zhang C, Agarwal A. Graphene reinforced metal and ceramic matrix composites: a review. *Int Mater Rev* 2016;62(5):241–302. <https://doi.org/10.1080/09506608.2016.1219481>.
- Ko K, Jin S, Lee SE, Lee I, Hong J-W. Bio-inspired bimaterial composites patterned using three-dimensional printing. *Compos Part B-Eng* 2019;165:594–603. <https://doi.org/10.1016/j.compositesb.2019.02.008>.
- Güler Ö, Bağcı N. A short review on mechanical properties of graphene reinforced metal matrix composites. *J Mater Res Technol* 2020;9(3):6808–33. <https://doi.org/10.1016/j.jmrt.2020.01.077>.
- Ren S, Hong Q, Chen J, He X, Qu X. The influence of matrix alloy on the microstructure and properties of (flake graphite + diamond)/Cu composites by hot pressing. *J Alloys Compd* 2015;652:351–7. <https://doi.org/10.1016/j.jallcom.2015.08.191>.
- Dong LL, Lu JW, Fu YQ, Huo WT, Liu Y, Li DD, et al. Carbonaceous nanomaterial reinforced Ti-6Al-4V matrix composites: properties, interfacial structures and strengthening mechanisms. *Carbon* 2020;164:272–86. <https://doi.org/10.1016/j.carbon.2020.04.009>.
- Mu XN, Cai HN, Zhang HM, Fan QB, Wang FC, Zhang ZH, et al. Uniform dispersion of multi-layer graphene reinforced pure titanium matrix composites via flake powder metallurgy. *Mater Sci Eng A-Struct* 2018;725:541–8. <https://doi.org/10.1016/j.msea.2018.04.056>.
- Lee B, Koo MY, Jin SH, Kim KT, Hong SH. Simultaneous strengthening and toughening of reduced graphene oxide/alumina composites fabricated by molecular-level mixing process. *Carbon* 2014;78:212–9. <https://doi.org/10.1016/j.carbon.2014.06.074>.
- Chen Y, Zhang X, Liu E, He C, Shi C, Li J, et al. Fabrication of in-situ grown graphene reinforced Cu matrix composites. *Sci Rep* 2016;6:19363. <https://doi.org/10.1038/srep19363>.
- Huang Y, Bazarnik P, Wan D, Luo D, Pereira PHR, Lewandowska M, et al. The fabrication of graphene-reinforced Al-based nanocomposites using high-pressure torsion. *Acta Mater* 2019;164:499–511. <https://doi.org/10.1016/j.actamat.2018.10.060>.
- Chen B, Shen J, Ye X, Jia L, Li S, Umeda J, et al. Length effect of carbon nanotubes on the strengthening mechanisms in metal matrix composites. *Acta Mater* 2017; 140:317–25. <https://doi.org/10.1016/j.actamat.2017.08.048>.
- Liu Q, He XB, Ren SB, Zhang C, Liu TT, Qu XH. Thermophysical properties and microstructure of graphite flake/copper composites processed by electroless copper coating. *J Alloys Compd* 2014;587:255–9. <https://doi.org/10.1016/j.jallcom.2013.09.207>.
- Jiang R, Zhou X, Liu Z. Electroless Ni-plated graphene for tensile strength enhancement of copper. *Mater Sci Eng A-Struct* 2017;679:323–8. <https://doi.org/10.1016/j.msea.2016.10.029>.
- Luo F, Jiang XS, Sun HL, Mo DF, Zhang YL, Shu R, et al. High thermal and electrical properties of electroless graphene films reinforced Cu matrix laminated composites. *J Alloys Compd* 2022:925. <https://doi.org/10.1016/j.jallcom.2022.166710>.
- Stepanov ND, Yurchenko NY, Tikhonovsky MA, Salishchev GA. Effect of carbon content and annealing on structure and hardness of the CoCrFeNiMn-based high entropy alloys. *J Alloys Compd* 2016;687:59–71. <https://doi.org/10.1016/j.jallcom.2016.06.103>.
- Xu H, Zang J, Yuan Y, Zhou Y, Tian P, Wang Y. In-situ assembly from graphene encapsulated CoCrFeMnNi high-entropy alloy nanoparticles for improvement corrosion resistance and mechanical properties in metal matrix composites. *J Alloys Compd* 2019;811. <https://doi.org/10.1016/j.jallcom.2019.152082>.
- Li Z, Pradeep KG, Deng Y, Raabe D, Tasan CC. Metastable high-entropy dual-phase alloys overcome the strength-ductility trade-off. *Nature* 2016;534(7606):227–30. <https://doi.org/10.1038/nature17981>.
- Wang MM, Tasan CC, Ponge D, Dippel AC, Raabe D. Nanolaminate transformation-induced plasticity–twinning-induced plasticity steel with dynamic strain partitioning and enhanced damage resistance. *Acta Mater* 2015;85:216–28. <https://doi.org/10.1016/j.actamat.2014.11.010>.
- Zhao M, Xiong DB, Tan Z, Fan G, Guo Q, Guo C, et al. Lateral size effect of graphene on mechanical properties of aluminum matrix nanolaminated composites. *Scripta Mater* 2017;139:44–8. <https://doi.org/10.1016/j.scriptamat.2017.06.018>.
- Zhang Q, Dong S, Ma S, Hou X, Yang W, Zhang Y, et al. Microstructure and compressive behavior of lamellar Al<sub>2</sub>O<sub>3</sub>/Al composite prepared by freeze-drying and mechanical-pressure infiltration method. *Sci Eng Compos Mater* 2020;27(1): 1–9. <https://doi.org/10.1515/secm-2020-0001>.

- [40] Shaga A, Shen P, Sun C, Jiang Q. Lamellar-interpenetrated Al–Si–Mg/SiC composites fabricated by freeze casting and pressureless infiltration. *Mater Sci Eng A-Struct* 2015;630:78–84. <https://doi.org/10.1016/j.msea.2015.02.012>.
- [41] Cao M, Xiong DB, Tan Z, Ji G, Amin-Ahmadi B, Guo Q, et al. Aligning graphene in bulk copper: nacre-inspired nanolaminated architecture coupled with in-situ processing for enhanced mechanical properties and high electrical conductivity. *Carbon* 2017;117:65–74. <https://doi.org/10.1016/j.carbon.2017.02.089>.
- [42] Ferraro C, Meille S, Réthoré J, Ni N, Chevalier J, Saiz E. Strong and tough metal/ceramic micro-laminates. *Acta Mater* 2018;144:202–15. <https://doi.org/10.1016/j.actamat.2017.10.059>.
- [43] Li D, Yang Z, Jia D, Duan X, He P, Yu J, et al. Spark plasma sintering and toughening of graphene platelets reinforced SiBCN nanocomposites. *Ceram Int* 2015;41(9):10755–65. <https://doi.org/10.1016/j.ceramint.2015.05.011>.
- [44] Estili M, Sakka Y. Recent advances in understanding the reinforcing ability and mechanism of carbon nanotubes in ceramic matrix composites. *Sci Technol Adv Mater* 2014;15(6):064902. <https://doi.org/10.1088/1468-6996/15/6/064902>.
- [45] Meng L, Hu X, Wang X, Zhang C, Shi H, Xiang Y, et al. Graphene nanoplatelets reinforced Mg matrix composite with enhanced mechanical properties by structure construction. *Mater Sci Eng A-Struct* 2018;733:414–8. <https://doi.org/10.1016/j.msea.2018.07.056>.
- [46] Shen L, Zhao Y, Li Y, Wu H, Zhu H, Xie Z. Synergistic strengthening of FeCrNiCo high entropy alloys via micro-TiC and nano-SiC particles. *Mater Today Commun* 2021;26. <https://doi.org/10.1016/j.mtcomm.2020.101729>.
- [47] Miller WS, Humphreys FJ. Strengthening mechanisms in particulate metal matrix composites. *Scripta Metall Mater* 1991;25(1):33–8. [https://doi.org/10.1016/0956-716X\(91\)90349-6](https://doi.org/10.1016/0956-716X(91)90349-6).